Towards Reliable mmWave 6G RAN: Reconfigurable Surfaces, Smart Repeaters, or Both?

Giuseppe Leone*, Eugenio Moro*, Ilario Filippini*, Antonio Capone*, and Danilo De Donno§

*ANTLab - Advanced Network Technologies Laboratory, Politecnico di Milano, Milan, Italy
§Milan Research Center, Huawei Technologies Italia S.r.l, Milan, Italy
Email: {giuseppe.leone, eugenio.moro, antonio.capone, ilario.filippini}@polimi.it, danilo.dedonno@huawei.com

***Abstract*—Mm-Wave 5G NR promises to provide unprecedented access throughput to mobile radio networks but comes with several challenges. Network densification is the only viable solution to increase robustness in front of link outages due to random obstacles. While Integrated-Access-and-Backhauling (IAB) architecture is commonly considered the enabling technology to reduce the cost of such dense deployments, Reconfigurable Intelligent Surfaces (RISs) and Smart Repeaters (SRs) are very recently emerging as promising tools to provide further capabilities to 6G networks in Smart Radio Environments.**

However, the impact of these devices on next-generation networks is yet to be fully understood. In this paper, we provide a first answer to the questions arising in the deployment of mmWave RAN equipped with SRs and RISs. By means of mathematical programming models for full network planning optimization, we produce optimal network layouts that we leverage to assess in which scenario, in which position, and with which configuration SRs and RISs can better improve the reliability of such networks.

I. Introduction

After the integration of mmWave into 3GPP specifications, both industry and academia are pushing towards effective deployments, which will solve the sub-6GHz spectrum shortage and deliver multi-gigabit throughputs [1]. Results are promising, but guaranteeing the reliability of large-scale High-Frequency (HF) Radio Access Networks (RAN) remains an open challenge. Indeed, HF propagation is easily impaired by those physical obstacles which are, on the other hand, transparent at sub-6GHz frequencies. Consequently, traditional RAN deployment paradigms that work well for low frequencies cannot generally provide the same level of reliability when applied to HF RAN. One critical difference is the necessity to deploy dense access networks to provide users with multiple backup radio links to be used in case of obstacle blockages [2]. However, simply installing a larger number of base stations would bring about potentially prohibitive deployment and management costs. As such, smarter alternative approaches based on different flavours of relaying techniques are currently being investigated to maintain high reliability levels at lower cost and complexity.

Among the solutions expected to take part in such heterogeneous RAN deployments, Integrated Access and Backhaul (IAB) presents the highest level of maturity, and it is indeed considered a key enabler of HF RAN [3]. IAB consists of a wireless multi-hop network where base stations and intermediate relay nodes exploit in-band backhauling to provide access connectivity to final users. In an IAB network, only a single expensive base station (IAB-donor) is directly connected to the core. In contrast, the rest of the network (IAB-nodes) exploits message relaying and routing capabilities to forward backhaul traffic. Since IAB nodes do not require wired connectivity, they can be manufactured and deployed at relatively lower costs, hence why they are considered a key technology for the cost-effectiveness of HF RAN.

Alongside IAB, the concept of Smart Repeater (SR) has been very recently proposed within the 3GPP [4] as a new type of network node built upon the classical RF repeater employed in 4G and lower generations. An SR is able to make use of some side control information to enable a more intelligent amplify-and-forward operation in a system with time-division duplex (TDD) access and beamforming capabilities [5]. From an operation point of view, SRs are expected to be integrated into IAB networks to inexpensively enlarge the single IAB cell footprint, thus mitigating the need for cell densification and further reducing the overall RAN deployment cost.

Finally, passive relaying for HF RAN through Reconfigurable Intelligent Surfaces (RISs) has been recognized as an extremely cost-effective technique to provide blockage resilience to mmWave RAN deployments [6]. RISs are described as passive planar structures whose electromagnetic properties can be controlled to reflect and focus impinging radio waves towards arbitrary directions. Thus, when properly configured, RISs can create alternative radio paths between a base station and a User Equipment (UE), effectively behaving as passive relays. Previous works have shown the effectiveness of such an approach both at the link level [7] and at the system level [8].

RIS and SR prototypes are still characterized by a low technological readiness level, and their overall impact on 6G networks is yet to be fully understood. Several fundamental questions, essential to drive their development, are still open: Can HF RAN benefit from RISs and SRs? Can RISs and SRs provide cost-effective performance improvement? In which scenario do they provide the most significant benefits?

Several works analyze the behaviour of such devices at link level [9], showing their effectiveness in augmenting throughput and connectivity in Non-Line-of-Sight (NLOS) conditions. However, only a few works investigate how those devices can be integrated at the network level. Most of them provide analyses of coverage and received power in random RIS deployments [10]–[13], while other works consider user-RIS association optimization in given deployments [14], [15]. Preliminary works study the best distance from the base

ISBN 978-3-903176-49-2 © 2022 IFIP

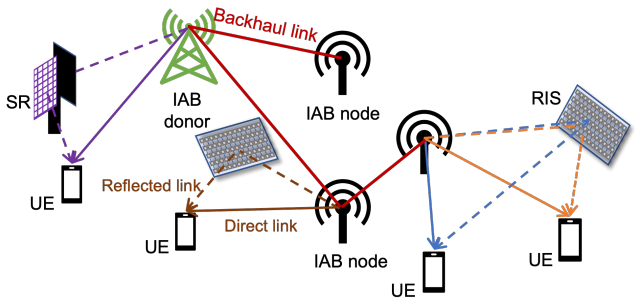

Fig. 1: HF RAN in Smart Radio Environment.

station at which RISs must be placed to maximize spectral efficiency [16] or minimize EMF exposure [17]. In [8], we provide a first study analyzing the impact of RISs in HF RAN planning, but, to the best of our knowledge, no work in literature proposes HF RAN planning methods where both SRs and RISs coexist with an IAB RAN architecture.

In this paper, we provide a first answer to the above questions on HF RAN equipped with SRs and RISs. By means of mathematical programming models for full network planning optimization, we produce optimal network layouts that we leverage to assess in which scenario, in which position, and with which configuration SRs and RISs can better contribute to improving the reliability of such networks.

The rest of the paper is structured as follows. Section II describes the network planning problem in smart radio environments with RISs and SRs. Section III details the formulation of the Mixed-Integer Linear Programming (MILP) model we have developed to optimize the layout of HF IAB networks when RISs and SRs are available, whose results are presented and discussed in Section IV. Section V concludes the paper with some final remarks.

II. Planning Smart Radio Environments

SRs and RISs can be installed alongside traditional RAN devices to improve the performance of radio access links by manipulating the radio propagation within the network's environment. From this perspective, they open a new era in wireless network optimization: the environment, traditionally considered the input of the optimization problem, now becomes an optimization variable. Indeed, the definition of Smart Radio Environment (SRE) [18] has been coined, referring to SRs and RISs as Smart radio Devices (SD). Similarly, a Smart Radio Connection (SRC) [6] identifies a triple of devices, including a transmitter, a receiver, and an SD (either a RIS or an SR) that aids the communication between the former two. An exciting application of SDs is to be designed as a way to provide UEs with natural dual-connectivity via alternative radio paths, which can be exploited to effectively reduce outages caused by obstacle obstructions in mm-Wave access networks.

RISs are typically modelled as *passive beamformers* [6], which can act on the radio propagation environment by focusing an impinging radio wave towards arbitrary directions. This capability can be exploited at the network level: through dedicated signalling, IAB-nodes are expected to dynamically command and change RIS configurations [19] to provide an alternative reflected path to connected users, following a time-division multiplexing approach.

Conversely, an SR is an *active* amplify-and-forward relay made by two back-to-back tunable phased-array panels that can operate in full-duplex mode. SRs enrich the radio propagation environment by enabling high-gain NLOS paths between UEs and IAB-nodes. Since they have the additional benefit of amplification, they typically provide higher bit-rates at the receiver than RISs. As in the case of RISs, SRs can be installed to establish reflected (and amplified) alternative paths for UEs.

However, both devices are subject to hardware limitations during their operations. RISs are characterized by a field-of-view in which both impinging and reflected radio-wave directions must be contained. SRs are a recent technological achievement that relies on sophisticated interference cancellation and isolation techniques between the two panels. Indeed, one panel is always active as a transmitter while the other simultaneously receives. While the cut-through mode reduces latency, full-duplex transmissions generate some limitations on the reciprocal orientation of the two SR panels. We will provide more details in the next section, where we will model SD's behavior.

SDs cooperate with mmWave IAB networks in a mmWave-RAN environment, as shown in Fig. 1. The IAB-donor is the only device connected to the core network with a wired link, and IAB-nodes form a wireless backhaul using mmWave frequencies. UEs get access via a mmWave link with either the IAB-donor or an IAB-node, which can route its traffic to the core network via multi-hop paths within the wireless backhaul. Backhaul links are established between IAB-nodes (or between IAB-node and the IAB-donor), while access links connect IAB-nodes (or the IAB-donor) to UEs. A distinguishing feature of mmWave IAB networks is that backhaul and access communications share the same frequency band (i.e., in-band backhaul).

An SRC (identified by links of the same colour in Fig. 1) provides two paths to connect IAB-nodes and UEs: a direct one and a reflected one, via its SD. Whenever a random obstacle suddenly appears and blocks the direct link between an IAB-node and a UE, SDs are essential to provide a reliable alternative path to support connectivity. This switch can occur very quickly, as the IAB-node just needs to steer its beam from the UE to the SD, while the SD is expected to be reconfigured on-the-flight through a fast and separated control plane. Moreover, since IAB-nodes and SDs are typically installed at places higher than UEs, we can realistically assume that backhaul and IAB-to-SD links are very rarely affected by random obstacles. Therefore, it is not convenient and a bit artificial to install SDs next to those links. For this reason, we do not consider blockages for them, apart from those given by fixed obstacles populating the geographic area. Instead, we do consider obstructions caused by random obstacles for links terminating as UEs, namely, direct links from UEs to

IAB-nodes and UE-to-SD links.

In order to make alternative paths an effective solution, a certain degree of uncorrelation between direct and reflected paths must be guaranteed during the network planning phase, which can be achieved by optimizing some geometric properties of the network layout. Previous works [20]–[22] have shown that access links with significant angular separation and small lengths can be very effective in mitigating random obstacle blockages. Indeed, a sizeable moving object could interrupt both direct and reflect paths if they are separated by a small angle at UE side. In addition, a large angular separation mitigates the self-blockage effect caused by the human body of the user [21]. The link length also influences blockage probability, as a longer radio connection will inherently have a higher probability of being blocked [22]. Additionally, short links can provide high bit-rates to UEs. Hence, the network planning formulation proposed in the next section will consider both aspects as metrics to identify good IAB network layouts.

III. HF RAN Planning Optimization

We begin this section by detailing the assumptions and the parameters that characterize the presented formulation. For the sake of clarity, we outline first a problem formulation that considers only downlink traffic demands; then, we will show in Sec. III-A the minor changes to apply for including uplink traffic as well.

As in many network planning works [20], [23], we consider a set $\mathcal{C}$ of Candidate Sites (CSs) over a geographic area covered by a mm-Wave access service. Each candidate site represents a position in which an IAB-donor, an IAB-node, or an SD can be installed. The UE distribution is modelled as an additional set of Test Points (TPs) $\mathcal{T}$. To simplify the model description, the set $\mathcal{I} = \{\text{RIS}, \text{SR}\}$ contains the different types of SD present in the network.

In order to create an SRC between a TP t, a CS c, and a SD r, we first need to verify whether its physical links can be established (f.i., devices are not too far or not obstructed by static obstacles). This is done by means of a binary activation parameter $\Delta^i_{t,c,r}$ set to 1 if an SRC can be crated between between TP $t \in \mathcal{T}$, an IAB-donor or an IAB-node installed in CS $c \in \mathcal{C}$ and an SD of type $i \in I$ installed in CS $r \in \mathcal{C}$. Since both RISs and SRs are instantly reconfigurable, as previously mentioned, they can participate in different SRCs at different times if the need occurs. However, in order to limit the complexity of both the separated control plane and the IAB network management [24], we believe it is reasonable to consider network layouts where each SD is associated with a unique IAB-node, which is in charge of controlling the SD. Hence, the same SD can be used to activate different SRCs to serve different UEs, provided they are all connected to the same IAB-node. Similarly to SRCs, we can define binary activation parameter $\Delta^{\text{BH}}_{c,d}$ that indicate whether two IAB-nodes in CSs c and d can establish a backhaul radio link.

Since mmWave communications are characterized by ultra-narrow beams at both transmitter and receiver, interference effects can be realistically neglected. Consequently, the capacity of both access and backhaul links can be pre-computed according to an arbitrary mmWave channel model once the scenario is given. Still referring to the SRC formed by a UE in TP t, an IAB-node in CS c, and a SD in CS r, the parameter $C^{\text{DIR}}_{t,c,r}$ represents the achievable direct-link access rate between the UE and the IAB-node, while $C^{\text{REF},i}_{t,c,r}$ indicates the rate of the reflected link through an SD of type i installed in CS r. Likewise, parameter $C^{\text{BH}}_{c,d}$ represents the capacity of the backhaul link between CSs c and d. A traffic demand D must be satisfied for each UE when using a direct link, while on the reflected link, only a fraction ξ, with $\xi \in [0, 1]$, of the demand is required, namely ξD. Note that by varying the *protection factor* ξ, we ask the planning for different network capacities. Indeed, when a blockage occurs, the network will reconfigure SRC's devices to maintain user connectivity, with a minimum guaranteed capacity defined by ξ.

Finally, network planning is assumed to have a limited budget B. Prices for each node type are included in the model via parameters $P^{\text{IAB}}, P^{\text{RIS}}, P^{\text{SR}}$. The cost of the unique IAB-donor is known and unavoidable. Hence it is not included in the optimization budget.

The formulation of the MILP (Mixed Integer Linear Programming) model for the mmWave-IAB-network planning problem with SDs is described in the following. The entire set of constraints has been split into a few homogeneous groups to simplify the exposition.

a) Deployment constraints: These constraints leverage binary decision variables y^{DON}_c, y^{IAB}_c, y^{RIS}_c, and y^{SR}_c, set to 1 if an IAB-donor, an IAB-node, an RIS, or an SR is respectively installed in CS $c \in \mathcal{C}$. Constraints (1) state that only one type of device, an IAB-node or an SD, can be installed in CS $c \in \mathcal{C}$, while constraints (2) and (3) state that a unique IAB-donor can be activated only in a CS assigned to an IAB-node (i.e., the IAB-donor is a special type of IAB-node). Constraint (4) sets a budget limit B for the entire network deployment.

$$y^{\text{IAB}}_c + y^{\text{RIS}}_c + y^{\text{SR}}_c \leq 1 \qquad \forall c \in \mathcal{C}, \quad (1)$$

$$y^{\text{DON}}_c \leq y^{\text{IAB}}_c \qquad \forall c \in \mathcal{C}, \quad (2)$$

$$\sum_{c \in \mathcal{C}} y^{\text{DON}}_c \leq 1, \quad (3)$$

$$\sum_{c \in \mathcal{C}} \left(P^{\text{IAB}} y^{\text{IAB}}_c + P^{\text{RIS}} y^{\text{RIS}}_c + P^{\text{SR}} y^{\text{SR}}_c \right) \leq B. \quad (4)$$

b) Topology constraints: We define binary activation variables $x^i_{t,c,r}$ for SRCs, which act as access links. They take value 1 if an SD of type $i \in \mathcal{I}$ in $r \in \mathcal{C}$ joins an SRC together with an IAB-node in $c \in \mathcal{C}$ and a UE in TP $t \in T$. Similarly, binary variables $z_{c,d}$ are set to 1 if the (directional) backhaul link connecting IAB-node in $c \in \mathcal{C}$ and IAB-node in $d \in \mathcal{C}$ must be established. Leveraging these variables, constraints (5) require to have $\Delta^{\text{BH}}_{c,d} = 1$ and a IAB-nodes installed in both CS c and CS d to activate backhaul link (c, d). Constraints (6) impose a spanning tree topology for the backhaul network (as indicated by 3GPP IAB

specifications [24]) by enforcing no more than one input link for each IAB-node, and none for the IAB-donor.

Similarly to the establishment of backhaul links, constraints (7) and (8) force all the devices in an active SRC to be actually installed. Since the aim of the network planning is to cover all TPs with an SRC to provide an alternative access link, constraints (9) enforce it, and allow to use either an RIS or an SR in the SRC.

Additional binary variables $s_{c,r}$ are defined to indicate with value 1 that an SD of any type installed in CS r is associated to (controlled by) an IAB-node in CS c. They are used in constraints (10) and (11) to limit the assignment of an SD to only one IAB node, while it can serve multiple TPs associated to the IAB node, as explained in the previous paragraphs.

$$z_{c,d} \leq \Delta^{\text{BH}}_{c,d} y^{\text{IAB}}_c, \quad z_{c,d} \leq \Delta^{\text{BH}}_{c,d} y^{\text{IAB}}_d, \qquad \forall c,d \in \mathcal{C}, \quad (5)$$

$$\sum_{d \in \mathcal{C}} z_{d,c} \leq 1 - y^{\text{DON}}_c, \qquad \forall c \in \mathcal{C}, \quad (6)$$

$$x^{\text{RIS}}_{t,c,r} \leq \Delta^{\text{RIS}}_{t,c,r} y^{\text{IAB}}_c, \quad x^{\text{RIS}}_{t,c,r} \leq \Delta^{\text{RIS}}_{t,c,r} y^{\text{RIS}}_r, \quad \forall t \in \mathcal{T}, c,r \in \mathcal{C}, \quad (7)$$

$$x^{\text{SR}}_{t,c,r} \leq \Delta^{\text{SR}}_{t,c,r} y^{\text{IAB}}_c, \quad x^{\text{SR}}_{t,c,r} \leq \Delta^{\text{SR}}_{t,c,r} y^{\text{SR}}_r, \quad \forall t \in \mathcal{T}, c,r \in \mathcal{C}, \quad (8)$$

$$\sum_{\substack{c,r \in \mathcal{C} \\ i \in \mathcal{I}}} x^i_{t,c,r} = 1, \qquad \forall t \in \mathcal{T}, \quad (9)$$

$$\sum_{i \in \mathcal{I}} x^i_{t,c,r} \leq s_{c,r} \qquad \forall t \in \mathcal{T}, \forall c,r \in \mathcal{C}, \quad (10)$$

$$\sum_{c \in \mathcal{C}} s_{c,r} \leq 1 \qquad \forall r \in \mathcal{C}. \quad (11)$$

c) Capacity constraints: In order to express capacity constraints, we introduce two new sets of fractional decision variables: variables $f_{c,d}$ indicating the backhaul traffic flow from the IAB-node installed in CS $c \in \mathcal{C}$ to the IAB-node installed in CS $d \in \mathcal{C}$ and variables $t^{\text{TX,ACC}}_c \in [0,1]$ that express the fraction of wireless resources allocated to access links at IAB-node in CS $c \in \mathcal{C}$. Note that the complementary resources fraction is dedicated to backhaul transmissions or left unused.

The flow crossing the backhaul is regulated by constraints (12), which state that the sum of the flows entering and exiting an IAB-node c must be equal to zero. Furthermore, the traffic coming from the core network can enter only an IAB-donor and is equivalent to the single UE demand D multiplied by the number of TPs $|\mathcal{T}|$. Constraints (13) are typical link-capacity flow constraints, which admit flows only for activated links.

Constraints (14) and (15) model wireless resource sharing at IAB-nodes. According to 3GPP specifications, IAB-nodes share their wireless resources (i.e., slots, symbols, time, etc.) among connected UEs and other IAB-nodes by scheduling access and backhaul transmissions, performed in half-duplex mode. We use a *link-utilization model* [25] to model resource sharing: to guarantee a rate D towards a receiver i using a link with a nominal capacity C_i, the transmitter has to occupy a fraction $\eta_i = \frac{D}{C_i}$ of its resources. This captures the effect of different spectral efficiencies caused by the different MCS selected according to experimented channel conditions. In order to obtain a feasible solution, the sum $\sum_i \eta_i$ over all the receivers of a transmitting IAB-node must be less or equal to 1, i.e., the transmitter cannot use more than 100% of its overall resources.

In constraints (14), we set the value of variable $t^{\text{TX,ACC}}_c$ equal to the overall wireless resources fraction that the IAB-node c dedicates to downlink access transmissions. Note that a UE can be alternatively served by either a direct link or a reflected link, each characterized by a required resource fraction. Therefore, the value of $t^{\text{TX,ACC}}_c$ at an IAB-node will be equal to the largest of the two, as we want to dimension the network capacity according to the most-demanding SRC configuration. IAB-node resource sharing is given in constraints (15), where resource fractions for backhaul transmission, backhaul reception, and access transmission are taken into account.

Resource sharing occurs at SDs as well, but the only shared resource is time and they are only involved in the establishment of reflected links. According to constraints (16), an SD can be part of multiple SRCs, and thus its activity time must be shared among them.

$$|\mathcal{T}| D y^{\text{DON}}_c + \sum_{d \in \mathcal{C}} (f_{d,c} - f_{c,d}) - \sum_{\substack{t \in \mathcal{T} \\ r \in \mathcal{C} \\ i \in \mathcal{I}}} D x^i_{t,c,r} = 0, \qquad \forall c \in \mathcal{C}, \quad (12)$$

$$f_{c,d} \leq C^{\text{BH}}_{c,d} z_{c,d}, \qquad \forall c,d \in \mathcal{C}, \quad (13)$$

$$t^{\text{TX,ACC}}_c = \sum_{\substack{t \in \mathcal{T} \\ r \in \mathcal{C} \\ i \in \mathcal{I}}} \max \left\{ \frac{D}{C^{\text{DIR}}_{t,c,r}}, \frac{\xi D}{C^{\text{REF},i}_{t,c,r}} \right\} x^i_{t,c,r} \qquad \forall c \in \mathcal{C}, \quad (14)$$

$$\sum_{d \in \mathcal{C}} \frac{f_{c,d}}{C^{\text{BH}}_{c,d}} + \frac{f_{d,c}}{C^{\text{BH}}_{d,c}} + t^{\text{TX,ACC}}_c \leq y^{\text{IAB}}_c \qquad \forall c \in \mathcal{C}, \quad (15)$$

$$\sum_{\substack{t \in \mathcal{T} \\ d \in \mathcal{C} \\ i \in \mathcal{I}}} x^i_{t,d,r} \frac{\xi D}{C^{\text{REF},i}_{t,d,r}} \leq y^{\text{RIS}}_r + y^{\text{SR}}_r, \qquad \forall r \in \mathcal{C}, \quad (16)$$

d) Smart Device Constraints: Two examples of SRCs with a RIS and a SR are shown in Fig. 2. An RIS is made of a single panel (surface) that presents a limited Field-of-view (FoV), like conventional planar antenna arrays [26], [27]. Hence, the orientation of a RIS needs to be such that both IAB-node and UE lines of sight fall in the RIS's FoV. On the other hand, an SR is made of two different adjustable panels, each characterized by an FoV. One panel of the SR must be oriented towards the IAB-node (IAB panel), and we can assume it can be perfectly pointed, while the other is oriented in the direction of UEs (UE panel). However, the two panels are not freely adjustable. In fact, a minimum angle of 90 degrees between the two panel directions must be guaranteed to make interference cancellation techniques effective, thus guaranteeing the sufficient isolation required for simultaneous transmission and reception. We consider only the FoV azimuthal angle F just for the sake of simplicity, but the formulation can be straightforwardly extended to include the FoV elevation angle. Finally, note that an RIS or a UE panel can be involved in multiple SRCs providing access to several UEs; therefore, the lines of sight to all these UEs must lie in the panel's FoV.

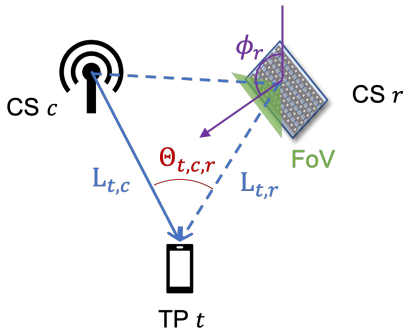

(a) SRC with RIS

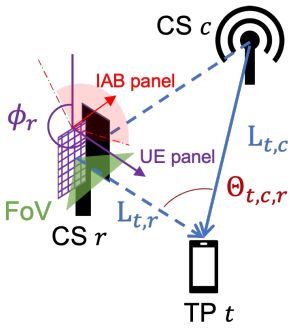

(b) SRC with SR

Fig. 2: The two types of Smart Radio Connection

Constraints (17) to (22) regulate the orientation of SDs. They rely on variables $\phi_r \in [0, 2\pi]$ that indicate the orientation (given a reference direction) of the SD installed in CS r. In case the SD is a RIS, ϕ_r is the orientation of its surface. In case the SD is a SR, ϕ_r is the orientation of the UE panel, as no choice must be made for the IAB panel, which is perfectly pointed towards the IAB-node. Parameters $\Phi^{\mathrm{A}}_{r,t}$ and $\Phi^{\mathrm{B}}_{r,d}$ store the angle (given the same reference direction) to TP t and, respectively, to CS d seen at CS r.

Constraints (17) and (18) state that the SD-UE link must fall in the FoV of the oriented SD (RIS surface or UE panel). If the SD is an RIS, the link from the IAB-node must lie in the same FOV as well, as enforced by constraints (19) and (20). If the SD is an SR, we define a 180-degree sector centered on the IAB panel's direction in which the UE panel cannot be oriented to avoid excessive interference. This is stated by constraints (21) and (22).

$$\phi_r \geq \Phi^{\mathrm{A}}_{r,t} - F/2 - 2\pi(1 - \sum_{i\in\mathcal{I}} x^i_{t,d,r}) \qquad \forall t \in \mathcal{T}, d, r \in \mathcal{C}, \quad (17)$$

$$\phi_r \leq \Phi^{\mathrm{A}}_{r,t} + F/2 + 2\pi(1 - \sum_{i\in\mathcal{I}} x^i_{t,d,r}) \qquad \forall t \in \mathcal{T}, d, r \in \mathcal{C}, \quad (18)$$

$$\phi_r \geq \Phi^{\mathrm{B}}_{r,d} - F/2 - 2\pi(1 - x^{\mathrm{RIS}}_{t,d,r}) \qquad \forall t \in \mathcal{T}, d, r \in \mathcal{C}, \quad (19)$$

$$\phi_r \leq \Phi^{\mathrm{B}}_{r,d} + F/2 + 2\pi(1 - x^{\mathrm{RIS}}_{t,d,r}) \qquad \forall t \in \mathcal{T}, d, r \in \mathcal{C}, \quad (20)$$

$$\phi_r \geq \Phi^{\mathrm{B}}_{r,d} + \pi/2 - 2\pi(1 - x^{\mathrm{SR}}_{t,d,r}) \qquad \forall t \in \mathcal{T}, \forall d, r \in \mathcal{C}, \quad (21)$$

$$\phi_r \leq \Phi^{\mathrm{B}}_{r,d} - \pi/2 + 2\pi(1 - x^{\mathrm{SR}}_{t,d,r}) \qquad \forall t \in \mathcal{T}, \forall d, r \in \mathcal{C}, \quad (22)$$

e) Objective Function: With the goal of striking the balance between the maximization of the direct-link vs reflected-link angular separation and the minimization of the average length of these links, we adopt the objective function:

$$\max \left\{ \mu \sum_{t\in\mathcal{T}} \frac{\theta_t}{\Theta} - (1-\mu) \sum_{t\in\mathcal{T}} \frac{l_t}{L} \right\} \quad (23)$$

The emphasis on one of the two aspects can be tuned by varying the parameter $\mu \in [0, 1]$. Note that considered values are normalized by constants $\Theta = 2\pi$ and L, the longest access link length in the network, to sum, for each TP, values in the $[0, 1]$ range.

The UE in TP t is served by a SRC characterized by the values of two variables: variable θ_t, which stores the angle between the direct link and the reflected link, and variable l_t, which stores the average lengths of direct and reflected links. The correct values of these variables are set leveraging parameters expressing the SRC topology, as shown in Fig. 2. Parameters $\Theta_{t,c,r}$ denote the smallest angle between two CSs c, r (the CS occupied by an SD or by an IAB is decided by the model) from the TP t's point of view, while parameters $L_{t,c}$ indicate the length of the link between TP t and CSs c. Constraints (24) and constraints (25) set the values of θ_t and l_t according to the SRC designed to serve TP t.

$$\theta_t \leq \sum_{c,r\in\mathcal{C},i\in\mathcal{I}} \Theta_{t,c,r}\, x^i_{t,c,r} \qquad \forall t \in \mathcal{T}, c, r \in \mathcal{C}, \quad (24)$$

$$l_t \geq \frac{1}{2} \sum_{c,r\in\mathcal{C},i\in\mathcal{I}} x^i_{t,c,r}(L_{t,c} + L_{t,r}) \qquad \forall t \in \mathcal{T}. \quad (25)$$

A. Uplink extension

The previous formulation can be extended to include the support of UE uplink transmissions. The main assumptions and constraints regulating node installation, budget, SRC establishment, assignment, and orientation remain the same. Angular separation and average link length aspects remain unaffected, together with the objective function. Only flow balancing and resource sharing constraints must be modified.

As for the flow balancing, we need to concurrently route uplink and downlink traffic flows within the backhaul. This is modeled by defining two sets of variables: $f^{\mathrm{UL}}_{c,d}$ for uplink traffic routed through link (c, d) and, similarly, $f^{\mathrm{DL}}_{c,d}$, which redefine variables $f_{c,d}$ for downlink traffic. Also, we define the minimum uplink demand D^{UL} to be guaranteed for each TP, while previously defined D becomes D^{DL}.

The following constraints replace capacity constraints in the previous section:

$$f^{\mathrm{DL}}_{c,d} + f^{\mathrm{UL}}_{c,d} \leq C^{\mathrm{BH}}_{c,d} z_{c,d}, \qquad \forall c, d \in \mathcal{C}, \quad (26)$$

$$|\mathcal{T}| D^{\mathrm{DL}} y^{\mathrm{DON}}_c + \sum_{d\in\mathcal{C}} (f^{\mathrm{DL}}_{d,c} - f^{\mathrm{DL}}_{c,d}) - \sum_{\substack{t\in\mathcal{T}\\ r\in\mathcal{C}\\ i\in\mathcal{I}}} D^{\mathrm{DL}} x^i_{t,c,r} = 0 \qquad \forall c \in \mathcal{C}, \quad (27)$$

$$-|\mathcal{T}| D^{\mathrm{UL}} y^{\mathrm{DON}}_c + \sum_{d\in\mathcal{C}} (f^{\mathrm{UL}}_{d,c} - f^{\mathrm{UL}}_{c,d}) + \sum_{\substack{t\in\mathcal{T}\\ r\in\mathcal{C}\\ i\in\mathcal{I}}} D^{\mathrm{UL}} x^i_{t,c,r} = 0 \qquad \forall c \in \mathcal{C}, \quad (28)$$

where constraints (26) state that the total traffic traversing link (c, d) must be limited by its capacity as in constraints (13). Following the same rationale as in constraints (12), constraints (27) enforce a per-node balance for downlink traffic, while uplink traffic is regulated by constraints (28). Two sets of uplink and downlink constraints are needed to avoid solutions where downlink traffic is balanced by an uplink short-circuit.

Introducing uplink traffic, we must consider both transmissions at UEs and receptions at IAB-nodes in resource sharing constraints. Similarly as before, we extend access links capacity to uplink and downlink directions. The new parameter $C^{(\text{UL, DIR})}_{t,c,r}$ $\left(C^{(\text{DL, DIR})}_{t,c,r}\right)$ represent the uplink (downlink) capacity of direct link, while parameter $C^{(\text{UL, REF}),i}_{t,c,r}$ $\left(C^{(\text{DL, REF}),i}_{t,c,r}\right)$ denotes the uplink (downlink) capacity when a SD of type i is installed.

In the formulation, constraints (14) are replaced by the following two constraints that consider access transmission and reception at the IAB-node in CS c:

$$t_c^{\text{TX,ACC}} = \sum_{\substack{t\in\mathcal{T}\\ r\in\mathcal{C}\\ i\in\mathcal{I}}} \max\left\{\frac{D^{\text{DL}}}{C^{(\text{DL, DIR})}_{t,c,r}}, \frac{\xi D^{\text{DL}}}{C^{(\text{DL, REF}),i}_{t,c,r}}\right\} x^i_{t,c,r} \qquad \forall c \in \mathcal{C}, \tag{29}$$

$$t_c^{\text{RX,ACC}} = \sum_{\substack{t\in\mathcal{T}\\ r\in\mathcal{C}\\ i\in\mathcal{I}}} \max\left\{\frac{D^{\text{UL}}}{C^{(\text{UL, DIR})}_{t,c,r}}, \frac{\xi D^{\text{UL}}}{C^{(\text{UL, REF}),i}_{t,c,r}}\right\} x^i_{t,c,r} \qquad \forall c \in \mathcal{C}, \tag{30}$$

Similarly, constraints (15) and (16) must be replaced by:

$$t_c^{\text{TX,BH}} = \sum_{d\in\mathcal{C}} \frac{f^{\text{DL}}_{c,d} + f^{\text{UL}}_{c,d}}{C^{\text{BH}}_{c,d}} \qquad \forall c \in \mathcal{C}, \tag{31}$$

$$t_c^{\text{RX,BH}} = \sum_{d\in\mathcal{C}} \frac{f^{\text{DL}}_{d,c} + f^{\text{UL}}_{d,c}}{C^{\text{BH}}_{d,c}} \qquad \forall c \in \mathcal{C}, \tag{32}$$

$$t_c^{\text{TX,BH}} + t_c^{\text{RX,BH}} + t_c^{\text{TX,ACC}} + t_c^{\text{RX,ACC}} \le y_c^{\text{IAB}} \qquad \forall c \in \mathcal{C}, \tag{33}$$

where constraints (31) and (32) capture the number of resources dedicated respectively to the downlink transmission and to the uplink reception at the IAB-node in CS c, while constraints (33) enforce half-duplex operations and resource sharing between backhaul and access at each IAB-node.

Finally, the same rationale can be used to extend SD resource sharing constraints (16) to include uplink operations:

$$\sum_{\substack{t\in\mathcal{T}\\ d\in\mathcal{C}\\ i\in\mathcal{I}}} x^i_{t,d,r}\left(\frac{\xi D^{\text{DL}}}{C^{(\text{DL, REF}),i}_{t,d,r}} + \frac{\xi D^{\text{UL}}}{C^{(\text{UL, REF}),i}_{t,d,r}}\right) \le y_r^{\text{RIS}} + y_r^{\text{SR}} \qquad \forall r \in \mathcal{C}. \tag{34}$$

IV. Results

In this section, we analyze the impact of RISs and SRs on HF RAN deployments. Leveraging the numerical results we obtained by applying the proposed network planning models to several instances, we evaluate the effect of SDs on angular separation and link length, which determine network robustness in front of obstructions caused by random obstacles. In particular, we want to identify the best combination of SDs that yields the best results in terms of reliability, considering different budgets and load conditions.

We produce random instances characterized by an area of $300\text{x}400m$ where 25 CSs and 15 TPs are randomly deployed. IAB nodes are modelled as 64-element linear-array antennas with a transmission power of $30dBm$ and carrier frequency set to $28GHz$. TPs are modelled as omnidirectional antennas. RISs are planar surfaces of $50\text{x}50cm$ containing 10^4 passive reflecting elements using a $\lambda/2$ inter-element spacing with a FoV of 120 degrees. SRs are modelled as active elements providing amplification. They provide a beamforming gain of $29dB$, and their UE-panel transmission power is set to $27dBm$. Pathloss and related datarates are calculated according to the channel models provided in [22].

Downlink TP traffic demand over direct links is set to $100Mbps$, while uplink demand is set to $10Mbps$. The normalized cost for an IAB node activation is set to $P_{IAB} = 1$. Deployment of RISs, being inexpensive with respect to IAB nodes, is performed by considering a normalized cost of $P_{RIS} = 0.1$. Smart Repeaters, being active elements, are more expensive than RISs, but are less expensive than IAB-nodes. Hence, we assume a SR deployment cost of $P_{SR} = 0.25$. All the results in this section are obtained by averaging 20 random drops of CS and TP positions. Random instances are generated in MATLAB and planning optimizations solved by CPLEX and each of them is typically solved in a time interval ranging from 3 to 15 minutes on an Intel Xeon(R) 2.40GHz server.

We compare three network planning strategies:

- RIS-only: Only IAB-nodes and RISs can be installed
- SR-only: Only IAB-nodes and SRs can be installed
- RIS+SR: The model can install both RISs and SRs together with IAB-nodes

Several works in literature ([8], [20]) have shown how access links characterized by large values of angular separation and short lengths can effectively provide high reliability to mmWave radio access networks in front of random obstacles. Moreover, the same works show how the optimal trade-off between angular separation and link length can be obtained by setting $\mu = 0.5$ in the objective function (23). Therefore, in the numerical evaluation, we mainly focus on the aspects strictly related to smart devices and their operations. We first discuss the planning trends emerging from the variation of the deployment budget B, then we analyze the impact of changing the protection factor ξ, i.e., changing reserved capacities on reflected links.

a) Deployment budget sensitivity: Fig. 3 shows the results in terms of angular separation, link length, and type of installed devices when the deployment budget changes from 2 to 11 units, while the protection factor ξ is fixed to 0.5. SR-only planning looks as the solution achieving the worst results in terms of geometrical properties. However, it possesses other advantages, as we will better explain in the second part of this

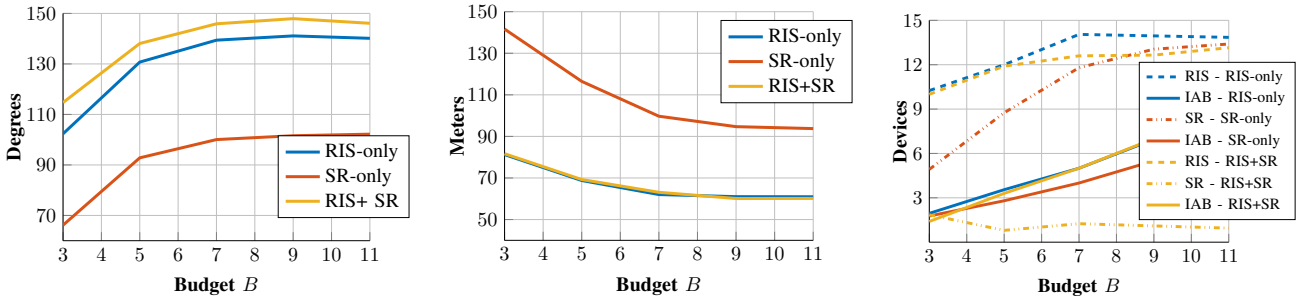

(a) Angular separation (b) Link length (c) Installed device

Fig. 3: Impact of different deployment budget (B) levels

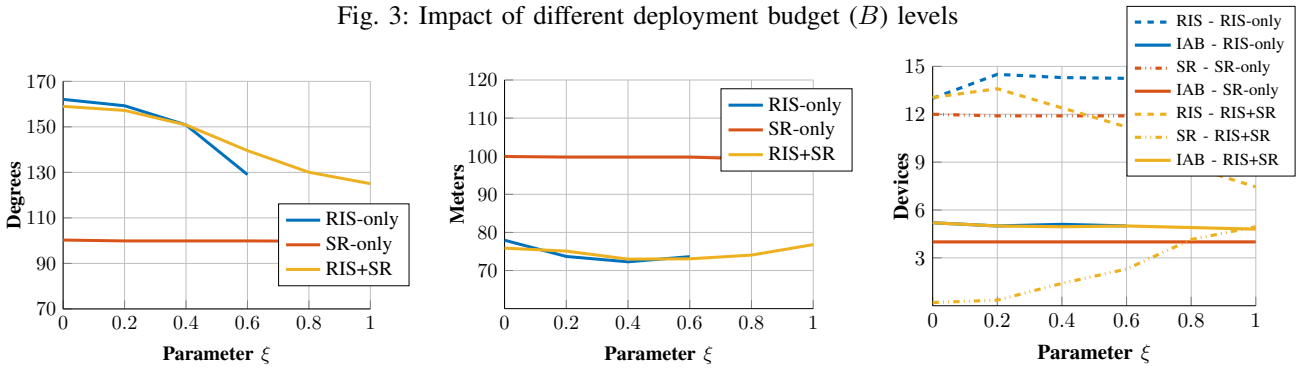

(a) Angular separation (b) Link length (c) Installed device

Fig. 4: Impact of protection factor (ξ) values

section. Vice versa, RIS+SR planning achieves the best results in angular separation and link length.

In Fig. 3c, we can note that more budget typically provides network layouts with more installed devices, which in turn leads to better results. The only exception is in RIS+SR planning with the number of installed SRs (dash-dotted yellow line): when B increases, the number of SRs does not significantly change. Indeed, the additional budget is preferably spent on more IAB-nodes. Again, the reason is that SRs are less effective than IAB-nodes in providing good angular separation. In order to better understand the reasons for this effect, we must analyze network layouts where capacity requests on reflected links change. We carry out this analysis by varying parameter ξ in the next section.

b) Protection factor sensitivity: In this second part of the numerical evaluation, we optimally plan random instances by varying the value of protection factor ξ in the range $[0, 1]$. In particular, $\xi = 0$ yields a network in which no demand is guaranteed on the reflected SRC link, while $\xi = 1$ imposes equal capacity on both direct and reflected links. In Fig. (4) we plot the average angular separation, the average link length, and the number of installed devices for the considered network scenarios. To carry out this analysis, we fix a deployment budget of 7 units, which is shown to be a reasonable value in the previous analyses.

Focusing on RIS-only results, we can note that for low values of ξ, it provides network layouts with large values of angular separation and short links. All the considered random instances can be optimally solved. On the other hand, for protection factors $\xi > 0.5$, the number of instances for which a feasible solution can be found decreases, while the angular separation is subject to a drastic reduction (Fig. 4a). In addition, for $\xi > 0.6$ very few or no solution can be found. Therefore, the RIS-only planning works only for small capacity guarantees on reflected links. This is due to the high path loss caused by signals bouncing on passive surfaces. RISs cannot support high MCSs; therefore, they require big wireless resource fractions that impact on the resource sharing constraints of both IAB-nodes and RISs. Hence, when ξ increases, the model tends to place RISs close to the TPs they can serve, yielding a negative impact on angular separation. This is further proved by decreasing link lengths in Fig. 4b. Hence, the results show that RIS-based planning is typically *capacity limited*.

Focusing now on the results of SR-only planning, we can notice that network layouts are characterized by small angular separation values and long links. This is due both to the limitations on the orientation of SR panels caused by interference cancellation requirements and to the SR signal amplification that can provide very high rates at long distances. Therefore, opposite to the case of RIS-only planning, SR-based planning is typically *topology limited*. This means that SRs are very effective in providing reflected links to UEs far from IAB-nodes, while RISs can optimally perform with close UEs.

Finally, the results show that planning with both RISs and SRs gives the best performance. Thanks to the possibility to optimally strike a balance between capacity and topology, network layouts can achieve the best angular separation and

link length for every value of ξ. As expected, increasing ξ also increases the network load, making network resources tight. Therefore, the absolute angular separation value tends to decrease with increasing ξ.

An interesting perspective is shown by Fig. 4c. When ξ grows, a constant number of SRs is installed in SR-only planning. Since capacity is not a limiting factor, SRs are insensitive to the increased request of network capacity. Moreover, the trends discussed in the previous paragraph are very evident: the results of RIS+SR plannig show that, when ξ increases, the number of installed RISs decreases as SRs replaces them to provide more capacity. The overall effect is that more SRs penalize the angular separation, as also shown by the decreasing RIS+SR curve in Fig. 4a.

V. Conclusion

6G HF RANs will operate in Smart Radio Environments where smart devices will improve network performances by manipulating the radio propagation. Robustness against obstacles is one of the essential features of mmWave RANs, and it can be remarkably improved by considering good access link alternatives since during the network planning phase. The impact on network planning of two recent types of smart devices, RISs and SRs, is not clear yet, but it is essential to understand their future development.

In this paper, we have presented MILP models to plan reliable mmWave 6G RANs equipped with RISs and SRs. These models can capture all the relevant aspects related to the installation and the operation of such devices. We have performed an extensive numerical analysis showing how relying on a single smart device can provide limited solutions in terms of either capacity or reliability. To capture the benefits of both RISs and SRs, we must jointly install them and strike a correct balance among them, like the one achieved by the proposed model.

Acknowledgment

The research in this paper has been carried out in the framework of Huawei-Politecnico di Milano Joint Research Lab. The authors acknowledge Huawei Milan research center for the collaboration.

References

[1] T. S. Rappaport, Y. Xing, O. Kanhere *et al.*, "Wireless communications and applications above 100 ghz: Opportunities and challenges for 6g and beyond," *IEEE Access*, vol. 7, pp. 78 729–78 757, 2019.

[2] M. N. Kulkarni, S. Singh, and J. G. Andrews, "Coverage and rate trends in dense urban mmwave cellular networks," in *2014 IEEE Global Communications Conference*, 2014, pp. 3809–3814.

[3] M. Polese, M. Giordani, T. Zugno *et al.*, "Integrated access and backhaul in 5g mmwave networks: Potential and challenges," *IEEE Comm. Mag.*, vol. 58, no. 3, pp. 62–68, 2020.

[4] Qualcomm, "RP-201139:New SID on Smart Repeaters for NR," 2020.

[5] Qualcomm, "RWS-210019: NR Smart Repeaters," 2021.

[6] E. Moro, I. Filippini, A. Capone, and D. De Donno, "Planning Mm-Wave access networks with reconfigurable intelligent surfaces," in *2021 IEEE 32nd Annual Int. Sym. on Personal, Indoor and Mobile Radio Comm. (PIMRC)*, Helsinki, Finland, Sep. 2021.

[7] P. Wang, J. Fang, X. Yuan, Z. Chen, and H. Li, "Intelligent reflecting surface-assisted millimeter wave communications: Joint active and passive precoding design," *IEEE Trans. on Vehic. Tech.*, vol. 69, no. 12, pp. 14 960–14 973, 2020.

[8] P. Fiore, E. Moro, I. Filippini, A. Capone, and D. De Donno, "Boosting 5G mm-wave IAB reliability with reconfigurable intelligent surfaces," in *2022 IEEE Wireless Communications and Networking Conference (WCNC) (IEEE WCNC 2022)*, Austin, USA, Apr. 2022.

[9] Q. Wu, S. Zhang, B. Zheng, C. You, and R. Zhang, "Intelligent reflecting surface-aided wireless communications: A tutorial," *IEEE Transactions on Communications*, vol. 69, no. 5, pp. 3313–3351, 2021.

[10] J. Kokkoniemi and M. Juntti, "Stochastic geometry based interference analysis of multiuser mmwave networks with ris," in *2021 IEEE 32nd Annual International Symposium on Personal, Indoor and Mobile Radio Communications (PIMRC)*, 2021, pp. 567–572.

[11] T. Hou, Y. Liu, Z. Song, X. Sun, Y. Chen, and L. Hanzo, "Mimo assisted networks relying on intelligent reflective surfaces: A stochastic geometry based analysis," *IEEE Transactions on Vehicular Technology*, vol. 71, no. 1, pp. 571–582, 2022.

[12] Y. Chen, B. Zhang, M. Ding, D. López-Pérez, and H. Zheng, "Performance analysis of wireless networks with intelligent reflecting surfaces," in *2021 IEEE Wireless Communications and Networking Conference (WCNC)*, 2021, pp. 1–6.

[13] J. Lyu and R. Zhang, "Hybrid active/passive wireless network aided by intelligent reflecting surface: System modeling and performance analysis," *IEEE Transactions on Wireless Communications*, vol. 20, no. 11, pp. 7196–7212, 2021.

[14] W. Mei and R. Zhang, "Performance analysis and user association optimization for wireless network aided by multiple intelligent reflecting surfaces," *IEEE Transactions on Communications*, vol. 69, no. 9, pp. 6296–6312, 2021.

[15] M. Aryan, H. A. H. Hassan, A. Nasser, and L. Nuaymi, "A new approach for user selection and resource management in intelligent reflected surface assisted cellular networks," in *2021 IEEE 94th Vehicular Technology Conference (VTC2021-Fall)*, 2021, pp. 1–7.

[16] C. You, B. Zheng, W. Mei, and R. Zhang, "How to deploy intelligent reflecting surfaces in wireless network: Bs-side, user-side, or both sides?" *Journal of Communications and Information Networks*, vol. 7, no. 1, pp. 1–10, 2022.

[17] H. Ibraiwish, A. Elzanaty, Y. H. Al-Badarneh, and M.-S. Alouini, "Emf-aware cellular networks in ris-assisted environments," *IEEE Communications Letters*, vol. 26, no. 1, pp. 123–127, 2022.

[18] M. Di Renzo, M. Debbah, D.-T. Phan-Huy *et al.*, "Smart radio environments empowered by reconfigurable ai meta-surfaces: An idea whose time has come," *EURASIP Jrn. on Wirel. Comm. and Networking*, vol. 2019, no. 1, pp. 1–20, 2019.

[19] R. Flamini, D. De Donno, J. Gambini, F. Giuppi, C. Mazzucco, A. Milani, and L. Resteghini, "Towards a heterogeneous smart electromagnetic environment for millimeter-wave communications: An industrial viewpoint," *IEEE Transactions on Antennas and Propagation*, 2022.

[20] F. Devoti and I. Filippini, "Planning mm-wave access networks under obstacle blockages: A reliability-aware approach," *IEEE/ACM Trans. on Networking*, vol. 28, no. 5, pp. 2203–2214, 2020.

[21] T. Bai and R. W. Heath, "Analysis of self-body blocking effects in millimeter wave cellular networks," in *2014 48th Asilomar Conf. on Signals, Systems and Comp.*, 2014, pp. 1921–1925.

[22] M. R. Akdeniz, Y. Liu, M. K. Samimi, S. Sun, S. Rangan, T. S. Rappaport, and E. Erkip, "Millimeter wave channel modeling and cellular capacity evaluation," *IEEE Jrn. on Sel. Areas in Comm.*, vol. 32, no. 6, pp. 1164–1179, 2014.

[23] E. Amaldi, A. Capone, M. Cesana, and I. Filippini, "Coverage planning of wireless sensors for mobile target detection," in *2008 5th IEEE International Conference on Mobile Ad Hoc and Sensor Systems*. IEEE, pp. 48–57.

[24] 3GPP, "NR; Study on integrated access and backhaul," Technical Specification (TS) 38.3874, 01 2019, version 16.0.0.

[25] S. Paris, F. Martignon, I. Filippini, and L. Chen, "An efficient auction-based mechanism for mobile data offloading," *IEEE Transactions on Mobile Computing*, vol. 14, no. 8, pp. 1573–1586, 2014.

[26] X. Tan, Z. Sun, D. Koutsonikolas, and J. M. Jornet, "Enabling indoor mobile millimeter-wave networks based on smart reflect-arrays," in *IEEE INFOCOM 2018*, 2018, pp. 270–278.

[27] J. Palacios, D. De Donno, and J. Widmer, "Lightweight and effective sector beam pattern synthesis with uniform linear antenna arrays," *IEEE Antennas and Wireless Propagation Lett.*, vol. 16, pp. 605–608, 2017.